STScI | SPACE TELESCOPE SCIENCE INSTITUTE

Instrument Science Report WFC3 2020-09

Updated Calibration of the UVIS G280 Grism

Nor Pirzkal

November 17, 2020

Abstract

We present the result of a full calibration effort of the WFC3 UVIS G280 slitless spectroscopic mode. We have combined all of the G280 calibration data (nearly 600 datasets) obtained over the years to determine the traces, wavelength calibration, and flux calibration across the entire field of view of both UVIS detectors, modelling the large amount of field dependence of the G280 grism. This was done for the $\pm 1, \pm 2, \pm 3,$ *and* $\pm\, 4$ *orders, and we have calibrated the position of the* 0^{th} *order as well.*

1. Introduction

The most recent calibration for the UVIS G280 grism was performed in 2017 (Pirzkal et al. 2017b). Before the 2017 calibration, the ± 1 orders had been calibrated only at the center of each UVIS detector. The new calibration of the trace and wavelength dispersion of the ± 1 orders were expanded to cover both detectors (CHIP1 and CHIP2). While a 2D field dependence was determined, it did not include higher spectral orders, nor did it include a re-calibration of the G280 sensitivity. The latter has thus remained unchanged since it was measured during ground testing using a micrometer.
New observations of a flux calibrator (GD-71) and a wavelength calibrator (WR14) have

since been obtained, by placing targets at additional locations on both detectors in order to provide a better sampling of the field dependence of the G280 grism (Calibration proposals 16022 and 16023). Here we summarize our effort to calibrate multiple spectral orders of the G280 grism. This work follows a methodology that is similar to that used in the past to calibrate the WFC3 IR G102 and G141 grisms (Pirzkal et al. 2016), and the WFC3 UVIS G280 grism (Pirzkal et al. 2017). All existing calibration observations of GD-71 and WR14 were used for this effort. While only the +1 and -1 orders are likely to be scientifically useful, we extended our calibration to include all of the spectral orders for which a spectral trace could be measured and fitted. We show an example of a full G280 spectrum in Figure 1.

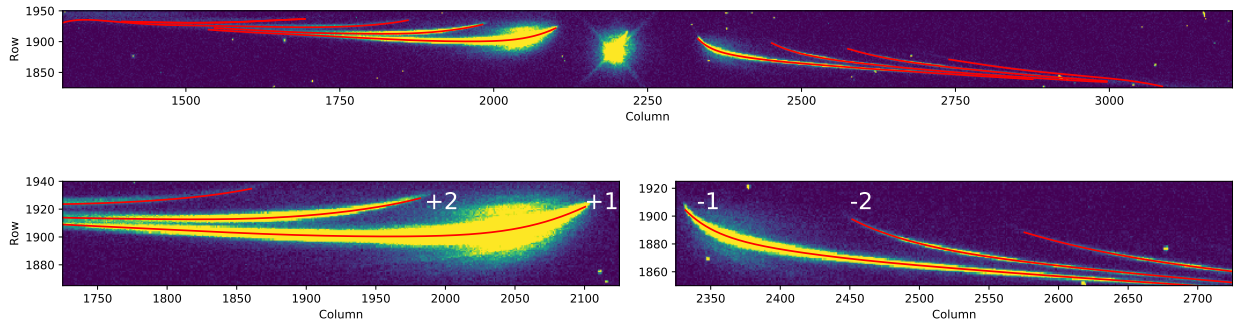

Fig. 1.—: The G280 spectrum of the White Dwarf GD-71 (Top Panel). Close-ups of the 1^{st} and 2^{nd} orders are shown in the bottom panels. The different spectral orders overlap significantly beyond the regions that are shown in the bottom panels.

2. Data

We used data from the 17 distinct UVIS G280 calibration programs that are listed in Table 1. These data include observations of the flux calibrator GD-71 (a white dwarf star at ICRS J2000 R.A.=05:52:27.62 Dec=+15:53:13.23 with an R magnitude of 13.169) and of the wavelength calibrator WR-14 (HD 76536, a Wolf Rayet star at ICRS J2000 R.A.=08:54:59.17 Dec=-47:35:32.66 with an R band magnitude of 9.52). The pool of data consists of a total of 595 observations, 335 of which use the G280 grism, 130 the F300X filter, and 130 the F200LP filter as well.

Table 1:: G280 Calibration Data

Program Numbers					
11934	11935	12359	12704	12705	13090
13091	13577	13578	14025	14026	14387
14545	14995	15588	16022	16023	14127[a]

[a]GO Program PI: Fumagalli, used for 0^{th} order calibration.

3. 0^{th} order

The G280 calibration data were obtained using a custom sub-array mode. Unfortunately, this introduced potential error in the estimated pointing of these observations. This problem was first identified by Rothberg et al. 2011, but has remained unfixed. Since measuring the characterization of the dispersion of slitless data is done with respect to the known position of the object in the field (as determined using short-exposure direct imaging data taken before or after a slitless observation), any pointing error introduced between the time the direct image and the slitless image are taken is a problem.

By first mapping the position of the 0^{th} order in G280 grism observations to the location of sources in the direct image, we can however determine the position of a target in a direct image from the position of the 0^{th} spectral order of the same target in the sliltess observation. Since the astrometry of the UVIS G280 calibration data, as well as the placement of the custom sub-array in the larger field of view were un-reliable, we had to rely on a different set of observations to calibrate this order. Fortunately, Data from GO Program 14127 (PI:Fumagalli) are well suited for this task since they were all obtained using full frame mode, and the corresponding direct images and slitless observations were obtained at the exact same pointing (i.e. without using dithering between the two). This enabled us to measure the position of the 0^{th} orders in 135 G280 observations and the position of the target in the corresponding F300X direct imaging. Since 0^{th} orders are nearly un-dispersed, we determine their positions, as well as the position of the target in imaging data using simple Gaussian fitting. For each imaging exposure, we identified as many sources ($\approx 5 - -10$ per detector) as possible (using the Python package `photutils`, which provided us with a good spatial coverage of both UVIS detectors (CCD1 and CCD2). In Figure 2, we show all of the positions that we used to calibrate the 0^{th} order. The calibration of the field dependence of this order is somewhat simpler than that of the other spectra orders since we can assume that the 0^{th} order is not dispersed. For each detector, we simply need to relate the position of a source in a direct image (x_{00}, y_{00}) to the position of the 0^{th} order in a dispersed image

(x_0, y_0). This was done by by modelling the difference between the two sets of coordinate as a function of the position of the target in the direct image $\delta_x(x_{00}, y_{00}) = x_0 - x_{00}$ and $\delta_y(x_{00}, y_{00}) = y_0 - y_{00}$. We approximated δ_x and δ_y as 2D polynomial functions:

$$f_{0,x}(x_{00}, y_{00}) = a_{0,x} + a_{1,x} \times x_{00} + a_{2,x} \times y_{00} + a_{3,x} \times x_{00}^2 + a_{4,x} \times x_{00} \times y_{00} + a_{5,x} \times y_{00}^2 \quad (1)$$

and

$$f_{0,y}(x_{00}, y_{00}) = a_{0,y} + a_{1,y} \times x_{00} + a_{2,y} \times y_{00} + a_{3,y} \times x_{00}^2 + a_{4,y} \times x_{00} \times y_{00} + a_{5,y} \times y_{00}^2 \quad (2)$$

We iteratively solved for the values of the parameters $a_{i,x}$ by fitting equations 1 and 2 to our set of measured positions, rejecting outliers. The final RMS of the fits is better than 0.3 pixels in both the x– and y– directions, for both the CCD1 and the CCD2 detectors, with good field coverage over both detectors. Figure 2 shows both the initial and final set of positions that we used as well as histograms of the residuals of the fit.

4. Traces

The ± 1 orders were re-calibrated in Pirzkal et al. 2017b at several positions on CCD1 and CCD2, but the spatial sampling of the data across the detectors was limited and the solution near the edges of the UVIS detectors was never directly measured and we had to instead rely on extrapolations of the derived field dependence. Moreover, higher spectral orders were never calibrated, making it difficult to estimate where the ± 1 spectral orders might have been contaminated by the ± 2 orders, for example. To calibrate the spectral traces of the spectral orders we could see in our data, namely the first four spectral orders, we began by manually measuring the (x,y) pixel coordinates of a dozen or so points along each spectral trace. This was done for all 335 available G280 datasets. As Figure 1 shows, the dispersed light of different spectral orders blends together at longer wavelengths and this provided a hard limit to how far into the red we could measure the spectral traces of the $\pm 1, \pm 2, \pm 3$, and ± 4 orders. This initial coarse manual sampling of the 8 spectral orders was then fitted using univariate splines. These fits were then used to automatically fit Gaussian profiles at each x– position along the spectral traces. While doing this, multiple Gaussian profiles were fitted simultaneously where more than one order was present (i.e. up to four). An additional linear component was also included to account for any background residuals. The fitting was performed using the `astropy.modeling` Python package and the FWHM of the separate Gaussian profiles were fixed to be the same for all spectral orders. These trace measurements were performed using all of the G280 observations of GD71 as well as

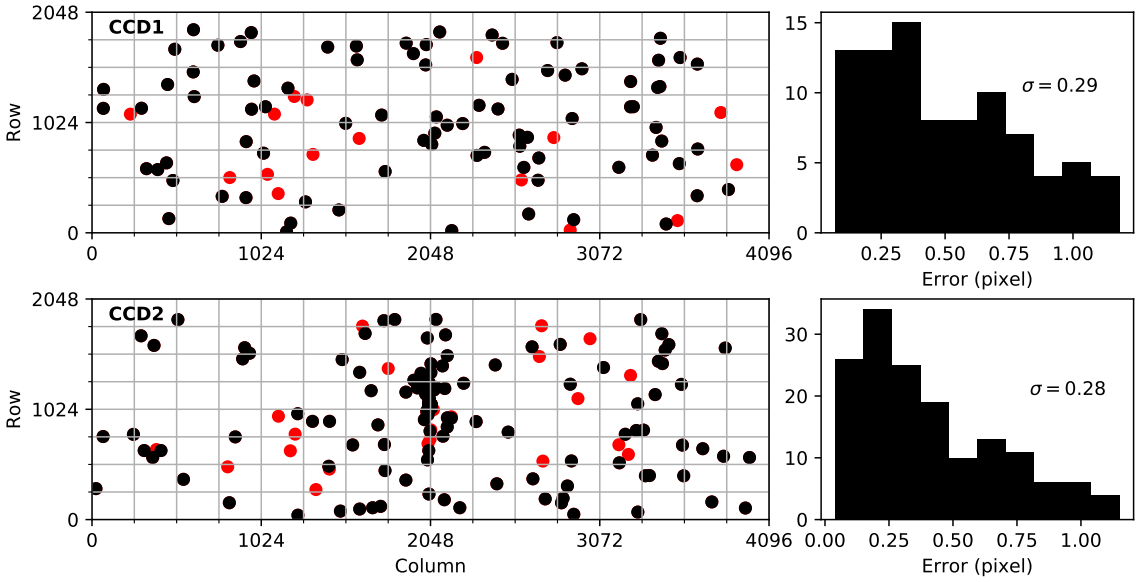

Fig. 2.—: Left Panels: Objects with measured positions in F300X direct imaging and with measured 0^{th} order positions in the associated G280 data from proposal GO-14127. Red points indicate the few locations that were iteratively rejected. CCD1 is shown on top and CCD2 is shown below. Right Panels: Histograms of the residuals between fitted and measured positions of the 0^{th} orders are shown. The residuals have standard deviations below 0.3 pixel.

the WR-14 observationsfrom the 17 G280 calibration proposals listed in Table 1. Figure 3 shows all of the individually measured traces for all of the 8 spectral orders. This figure demonstrates the large variation in the positions and shapes of the traces over each detector as different measurements of the trace of particular spectral orders do not overlap and are offsets by several pixels. As there is a lot of variation on the redder ends of these traces, we first median-combined all traces that were in the same vicinity (within 100 pixel), using an iterative sigma clipping procedure to remove bad observations ($\approx 16\%$). The individual target positions as well as the positions where we computed median traces are shown in Figure 4. Field-dependent models of these median spectra traces were estimated using the method discussed in Pirzkal et al. 2016 using the more generalised parametrization of Pirzkal et al. 2017a. To summarize, the traces were calibrated by fitting 2D field polynomials that define $\delta_x = x' - x_{00}$ and $\delta_y = y' - y_{00}$ as a function of a free parameter called t (details are

available in Pirzkal et al. 2017a).

$$\delta_x = x' - x_{00} = f_x(x_{00}, y_{00}; t) \tag{3a}$$

$$\delta_y = y' - y_{00} = f_y(x_{00}, y_{00}; t) \tag{3b}$$

where f_x and f_y are 2^{nd} order 2D polynomials describing an n^{th} order polynomial traces of the form

$$P_{2,n}(x_{00}, y_{00}; t) = \sum_{i=0}^{n} t^i \times (a_{i,0} + a_{i,1} \times x_{00} + a_{i,2} \times y_{00} + a_{i,3} \times x_{00}^2 + a_{i,4} \times x_{00} \times y_{00} + a_{i,5} \times y_{00}^2) \tag{4}$$

Here, the free variable t was chosen so that t takes on values between 0 and 1 starting from lower wavelengths of the dispersed order (where the traces curl sharply upward) and ending at higher wavelengths (where the traces visually appear more linear and start to blend together). Figure 3 shows that the traces have a highly non linear shape on their bluer side, especially for the ± 1 and ± 2 orders, so a high order polynomial was used to fit the shape of these spectral traces. Our models allow one to reproduce the shape of the spectral traces of all 8 orders up to where spectral orders begin to contaminate one another. An example of the traces computed using this field dependent model is shown in Figure 5 where we show all 8 spectral orders for sources that are at the center of each detector, with the value of the free parameter t also shown. Polynomial orders of 14, 10, 8, and 5 were used for the $\pm 1, \pm 2, \pm 3$, and ± 4 spectral orders, respectively. Once this first set of models was determined for each order, we proceeded to automatically re-measure all of the spectral traces using the same fitting algorithm described above but with a tightened constraint on the y- position of the peak of each of the spectra orders. This provided a slight improvement in the quality of the trace measurements at low (i.e. blue end) and high (i.e. red) ends of spectral orders. This final set of measured traces was then fitted again using the same 2D polynomials shown above to compute field dependent models of the traces that can be computed as a function of the free parameter t. Good modelling of the spectral traces is essential since both the wavelength and flux calibration depend on them. In Figure 6 we show the residuals of the fit as a function of t. As this Figure shows, the 1^{st} and 2^{nd} order fits are within 0.5 pixel over the entire length of the trace. It is worth noting that the errors are well within 0.25 pixel over a significant fraction of the 1^{st} order trace. Note that, when expressed as a function of t, the 1^{st} and 2^{nd} orders become blended at $t > 0.7$ while the 3^{rd} and 4^{th} become blended at $t > 0.5$. We furthermore show in Figures 7 and 8 that we see no field dependence to the quality of the fit (as measured by the RMS between measurements and fit at $0.1 < t < 0.4$), demonstrating that the field modeling of the spectral traces over both detectors is good.

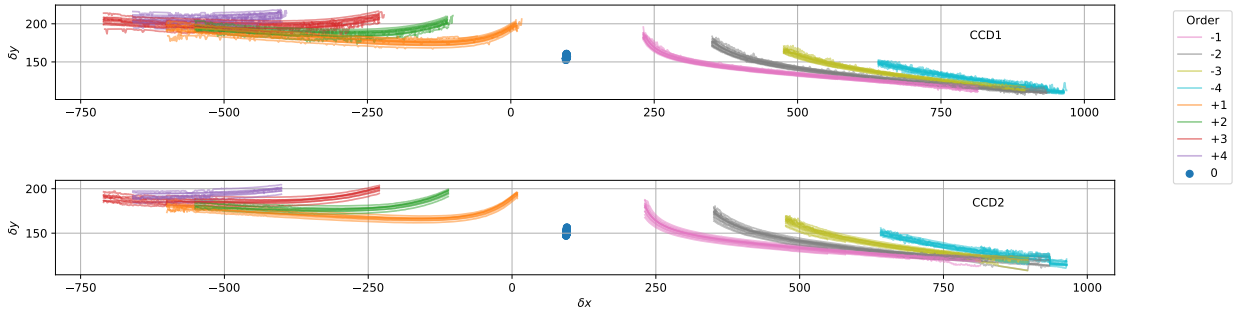

Fig. 3.—: This plot shows the measured traces of all of the spectral orders we calibrated, plotted as a function of the original source location x_{00}, y_{00} (which in this Figure is therefore at coordinates (0,0) and outside of the plotting areas). As this Figure shows, there is a large amount of field dependence in the shape of the traces as demonstrated by the large variation in the relative position and shape of each of the spectral orders. The apparent width of the spectral orders shown here is the direct result of the large variation of the relative positions and shape of the spectral traces over the field of view.

5. Wavelength

The G280 grism was wavelength-calibrated using the observations of our wavelength calibrator WR-14 in the G280 proposals listed in Table 1. We relied on the trace calibration described in Section 4, and extracted narrow 1D spectra of the $\pm1, \pm2, \pm3$, and ±4 from each observation. Extraction of the spectra of each observation was performed by using our field dependent models of the traces to compute where the traces were. A narrow (2–4 pixel wide) box extraction was then performed in the cross dispersion. This was done throughout the length of each order and therefore as a function of the free parameter t. In Pirzkal et al. 2017, we used the spectra from Willis et al. (1986) and Crowther et al. (2002) to estimate the fiducial wavelength of emission lines we observed in our G280 spectra, at wavelengths ranging from $1900 < \lambda < 8000\mathring{A}$. We used the same emission lines list in this work, and these are listed in Table 2.

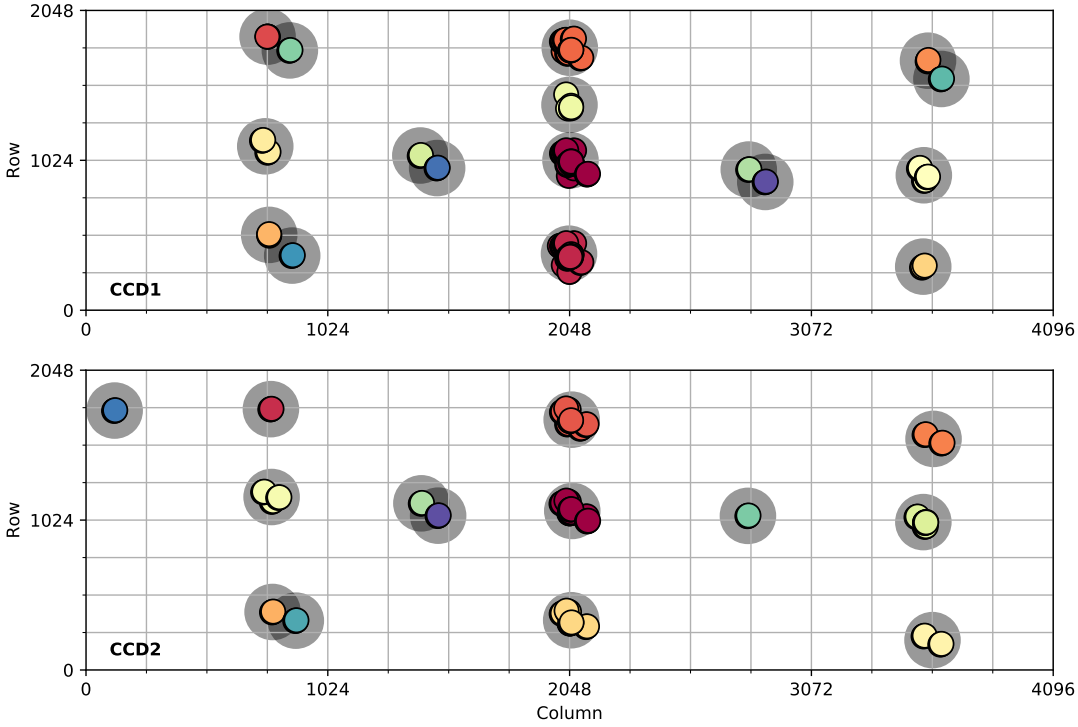

Fig. 4.—: Positions in each detector where traces were individually measured (smaller colored circles) and the positions at which median combined, higher signal to noise trace estimates were computed (larger grey circles).

Table 2:: Fiducial Emission Lines Wavelength for WR14

Emission Line Centers ($\AA$)					
1643.9	1911.0	2299.2	2402.6	2527.4	2906.0
3067.0	3400.0	3704.8	3932.9	4073.7	4334.2
4444.0	4654.6	5131.1	5813.4	6569.7	6744.9
7059.7	7218.8	7729.0			

Fiducial emission line wavelengths used to calibrate the UVIS G280 observations. These lines were measured from the spectra of Willis et al. (1986) and Crowther et al. (2002).

For each of the 8 orders in each of the 164 WR-14 observations, we identified a few prominent lines on the blue and red sides of the spectrum. The line positions, as a function of the free parameter t, were estimated by fitting a Gaussian profile to the core of the emission lines.

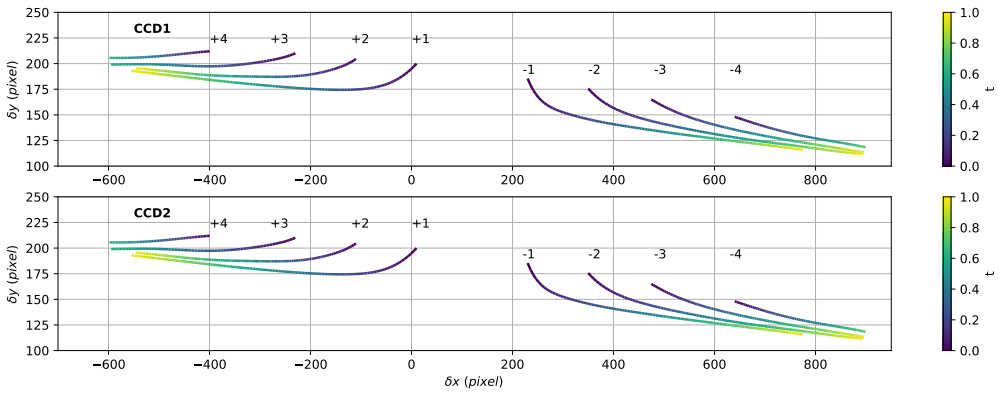

Fig. 5.—: Plot of the traces for an object at the center of CCD1 and CCD2. The traces shown here were computed from our 2D fit of all 8 spectral orders, as a function of the free parameter t, which we used to color code each spectral trace.)

These measurements were then used together with the fiducial wavelengths of these emission lines to determine an approximate wavelength solution $f(t) = \lambda$. This initial wavelength relation was then used to fit the observed position of every emission line shown in Table 2 (extending as far into the red as the spectral orders allowed). We fitted emission lines with wavelengths ranging from $> 1900\mathring{A}$ and $\lesssim 8000\mathring{A}$,$\lesssim 6000\mathring{A}$,$\lesssim 3400\mathring{A}$, and $\lesssim 3000\mathring{A}$ in spectral orders $\pm 1, \pm 2, \pm 3$, and ± 4, respectively. Figure 9 shows one instance of an extracted 1^{st} order spectrum, as a function of t, as well as the emission lines that were fitted and the center positions (expressed as values of t) of emission lines were measured in approximately 100 spectra, split nearly evenly between CCD1 and CCD2.

Modeling the field dependence of the wavelength calibration was done in a similar manner to our earlier modelling of the field dependence of the spectral traces.

A 2D polynomial was used to simultaneously fit our observations of x_{00}, y_{00}, t, and λ, using

$$\lambda = f_\lambda(x_{00}, y_{00}; t) \tag{5a}$$

where $f_\lambda(x_{00}, y_{00}; t)$ is 2D polynomial of the same form as Equation 4. Good fits were obtained using polynomial orders of 6, 4, 3, 2 for the $\pm 1, \pm 2, \pm 3$, and ± 4, respectively. We obtained overall good fits over the whole CCD1 and CCD2 detectors for all 8 spectral orders. While the ± 3 and ± 4 orders are faint, appear out of focus and have too limited of a wavelength range to be scientifically useful, the ± 1 and ± 2 wavelength solutions are accurate to within a small fraction of the nominal $10\mathring{A}$ resolution element ($\approx 3\ \mathring{A}$ and $\approx 4\ \mathring{A}$ for ± 1 and ± 2, respectively). Figures 10 to 13 show the residuals of the fit as a function of wavelength for

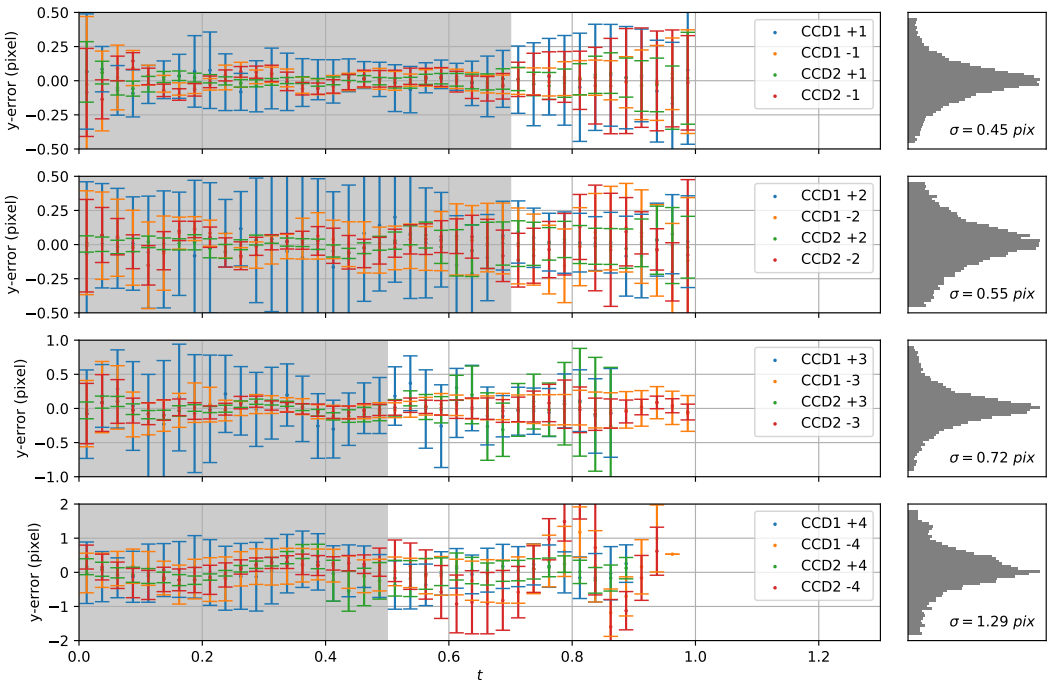

Fig. 6.—: Left Panels: Plot of the residuals of the fit of the spectral trace for the $\pm 1, \pm 2, \pm 3, \pm 4$ orders as a function of t. The grey shaded regions show the range where the spectra orders do not overlap with another spectral order. Right Panels: Histograms of the residuals.)

all 8 orders on both detectors. We show multiple extractions of the ± 1 spectral orders in Figure 14 to visually demonstrate the quality of the trace and wavelength calibration.

6. Flux

The flux calibration of the G280 grism has has not been revised since its initial estimate for the center of CCD1 and CCD2 in Kuntschner et al. 2009. These early measurements were based on monochromator measurements. This ISR represents the first attempt to derive the observed sensitivities of G280 from actual in-space observations. Having freshly calibrated the traces and wavelength solutions of all orders, from ± 1 to ± 4 we estimated the spectral-order sensitivities of the G280 on CCD1 and CCD2. The sensitivity curve for each

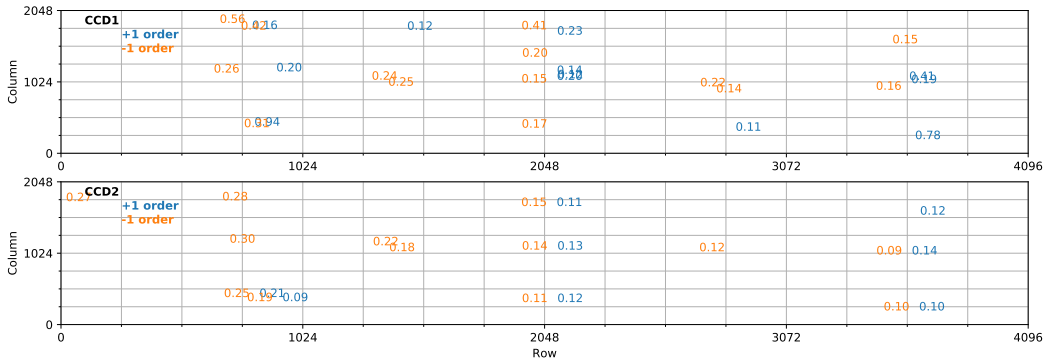

Fig. 7.—: Residuals to the 2D field dependence fit, computed at $0.1 < t < 0.4$, of the +1 (orange) and of the −1 (blue) spectral traces in CCD1 (Top Panel) and CCD2 (Bottom Panel).)

order can be estimated by dividing the known flux of the source at a given wavelength, by the number of e^-/s measured at that wavelength (divided by the bin width to express our observed count rate to be per $\mathring{A}$). In the case of GD-71 and the G280 grism and since orders are so close together in the cross-dispersion direction, we estimated the total observed flux as a function of wavelength by fitting Voigt profiles (The convolution of a Cauchy-Lorentz distribution and a Gaussian distribution) in the cross-dispersion direction, as we found that the Voigt profile provided an excellent fit to the cross dispersion shape of the spectral orders. At a given column, i.e. wavelength, up to four Voigt profiles were fitted simultaneously, with the addition of a linear component to account for a background signal. The FWHM and Gaussian kernel width of the Voigt profiles were constrained to be equal. The total observed count rate at that wavelength was then estimated by computing the integral of these Voigt profiles. Figure 15 shows an example, and we show the simultaneous fitting of a +1 and of a +2 spectral-trace profiles using a Gaussian, a Lorentz, and a Voigt profile, for comparison. Measuring the count rates for the ±1 orders using a classical box extraction, we found that an extraction width of ±40 pixels was required to include both the core and extended structure in the cross dispersion, clearly visible only in the blue parts of the ±1 orders. Such a wide extraction width is not practical since such a wide aperture can encompass multiple spectral orders, but we note that the count rate estimated using a Voigt profile correspond to 95% of the total flux (when using a very large aperture 80 pixels wide).

The flux calibrator GD-71 was observed over the entire field of view of CCD1 and CCD2 , and we allow for a variation of the G280 sensitivities by estimating the observed spectral orders of GD-71 at different positions. This is similar to what we did while computing the spectra traces of each spectral order in Section 4. Figure 16 shows the locations where we

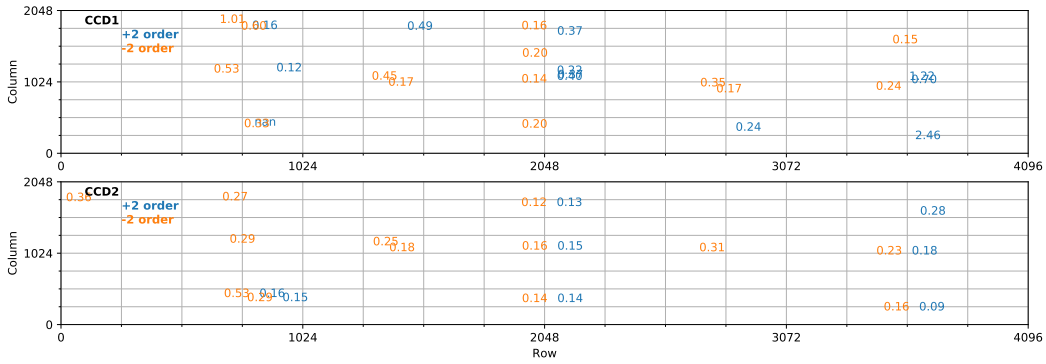

Fig. 8.—: Residuals to the 2D field dependence fit of the +2 (orange) and of the −2 (blue) spectral traces in CCD1 (Top Panel) and CCD2 (Bottom Panel).

median combined the extracted 1D spectra of each spectral orders. As was the case for our trace estimates, computing the median of a few observations taken at similar positions over the detectors allowed us to make these estimates more robust. We show the reference spectrum of GD-71 in Figure 17 and, as this Figure shows, the flux of this source decreases by a factor of about 100 from 2000$\mathring{A}$ to 8000$\mathring{A}$, which contributes to the difficulty of deriving a sensitivity function at redder wavelengths, which is also where spectra start to contaminate one another and is also the limit of where we could measure the traces of individual spectral orders.

In Figures 18 to 21 we show the extracted combined spectra of the $\pm1, \pm2, \pm3$, and ±4 spectral orders. Each of these Figures shows the positive and negative orders for CCD1 and CCD2. The error bars show the RMS in the measured count rate as the source was observed at the 10 (11) locations on CCD1 (CCD2), which are shown in Figure 16. While we showed extraction of the flux calibrator GD-71 for all 8 orders, the 3^{rd} and 4^{th} order-extractions suffer from a large amount of un-corrected contamination on the red end as well as large systematic errors in the case of the 4^{th} order (as this is the order for which both trace and wavelength solutions are the least reliable).

We used the STScI CALSPEC (Bohlin et al. 2014) model spectrum of GD-71 to derive the sensitivity curves of each spectral order up to the point where contamination from a higher order intrudes. Our empirically determined sensitivity estimates are shown in Figure 22. We also show the older, existing sensitivities derived during ground testing of the instruments and using a micrometer (Kuntschner 2009). As this Figure shows, the sensitivities derived for the ±1 and ±2 orders vary significantly between CCD1 and CCD2, while our CCD1 sensitivity estimates match the TV3 estimates reasonably, especially if one considers

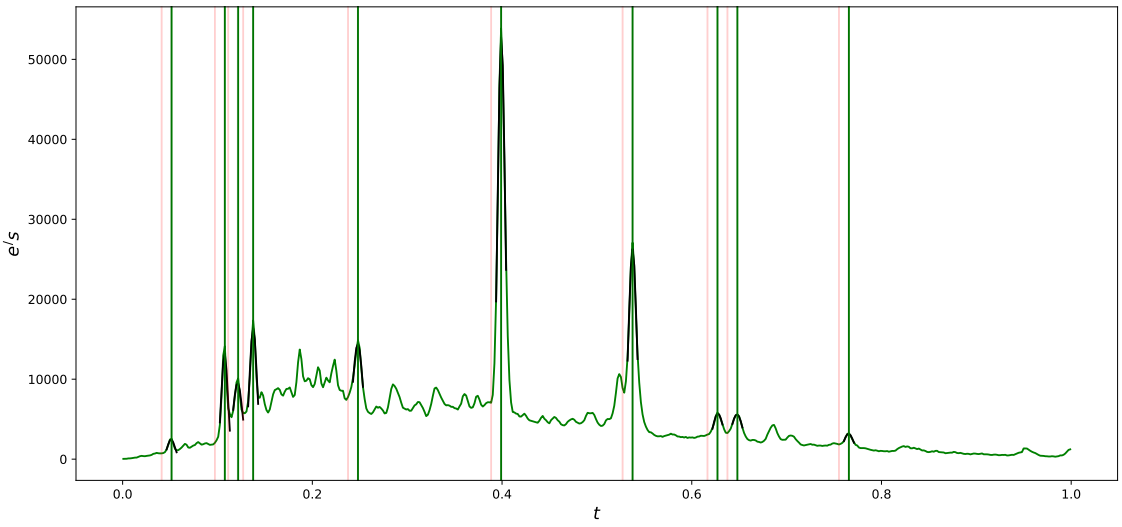

Fig. 9.—: One of our extracted 1^{st} order spectra of the WR-14 wavelength calibrator (in green). Emission lines from Table 2 are marked using vertical lines and we also show the Gaussian fit to the core of these lines (in black).

how differently the two estimates were derived. While we show the sensitivities we derived for ± 3 and ± 4 we caution that the faintness of these spectral orders, and the large uncertainties in our modelling of their spectral traces and wavelength dispersion add up to making these sensitivity estimates more qualitative rather than quantitative.

7. Conclusion

We have re-calibrated the UVIS G280 grism using all available data obtained since it was installed on HST. These provide a better spatial coverage of both UVIS detectors. We have measured and modelled the spectra traces and wavelength dispersion of the $\pm 1, \pm 2, \pm 3$, and ± 4 spectral orders, as well as the field dependent position of the 0^{th} order. Over the wavelength range where spectral orders do not overlap, our model of the field-dispersion of the spectral traces is accurate to within a fraction of a pixel. Similarly, our models of the wavelength solutions are accurate down to a small fraction of dispersion resolution. We have also empirically derived, for the first time since WFC3 was installed, the flux sensitivities of these eight spectral orders.

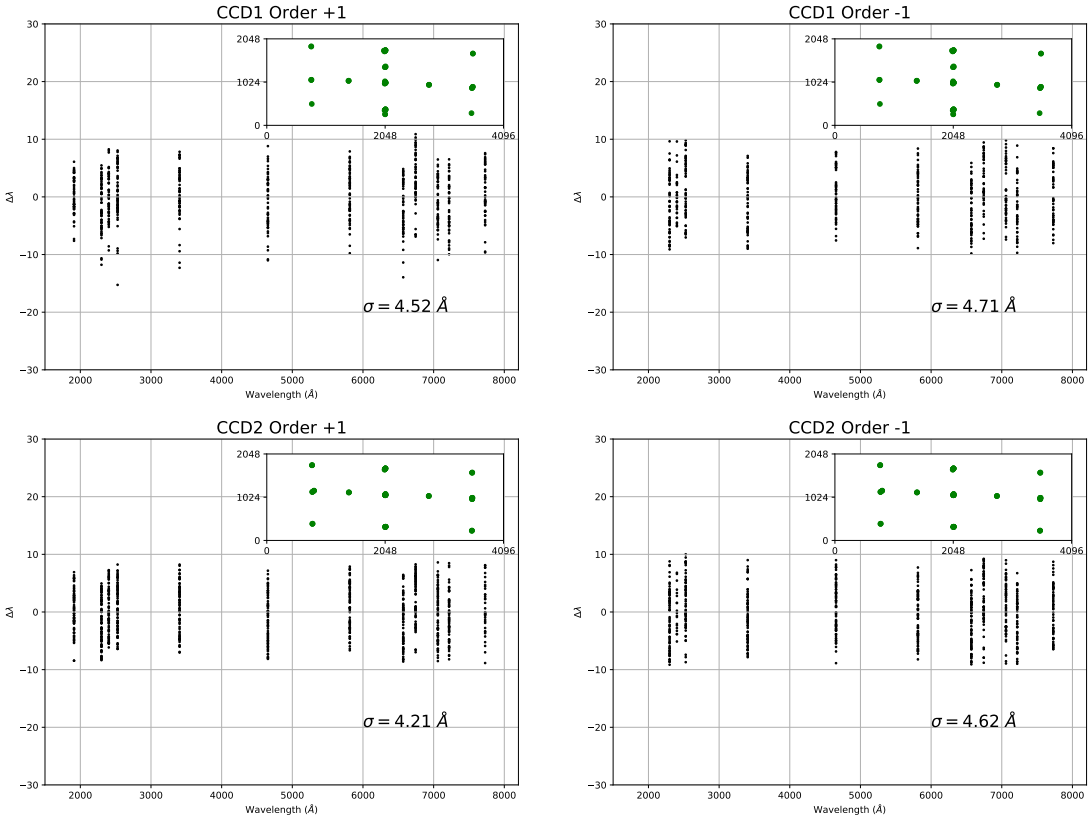

Fig. 10.—: The residuals of our new field dependent wavelength calibration, shown as a function of wavelength. Overall, we estimate the error in our new wavelength calibration to be ≈ 4 $\mathring{A}$. The inset plot shows the location on the detectors where the wavelength was calibrated.

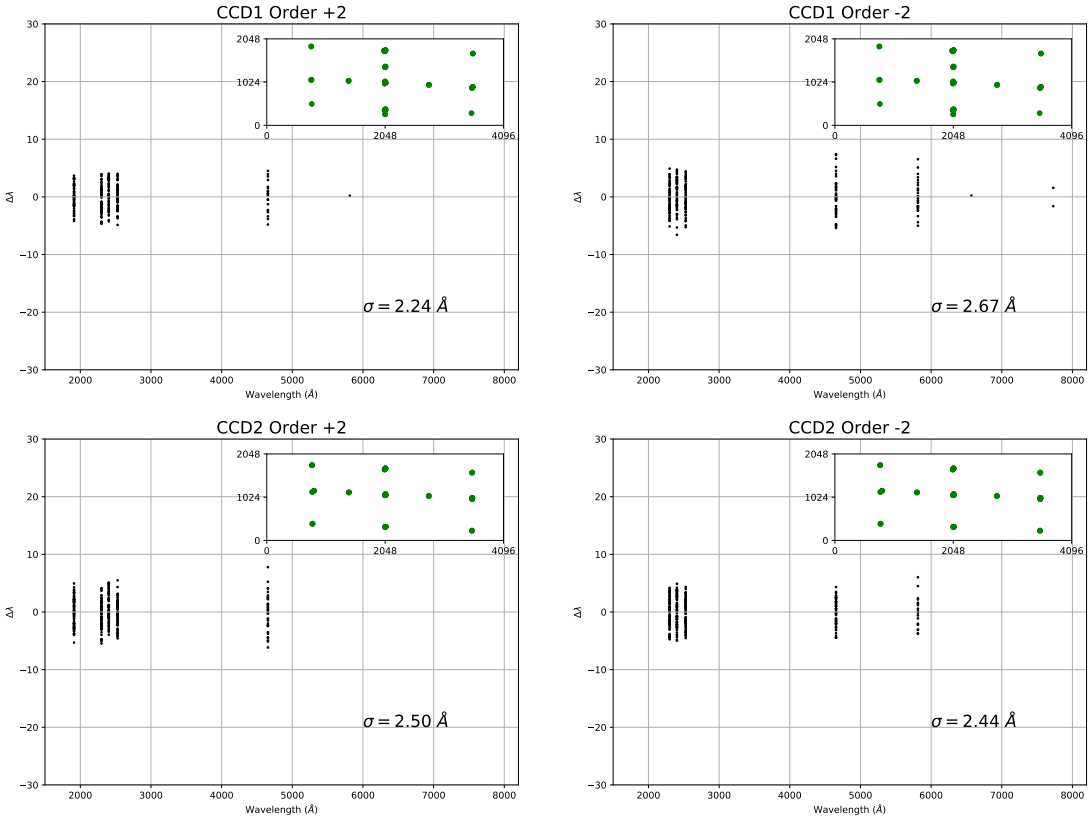

Fig. 11.—: The residuals of our new field dependent wavelength calibration, shown as a function of wavelength. Overall, we estimate the error in our new wavelength calibration to be ≈ 3 $\mathring{A}$. The inset plot shows the location on the detectors where the wavelength was calibrated.

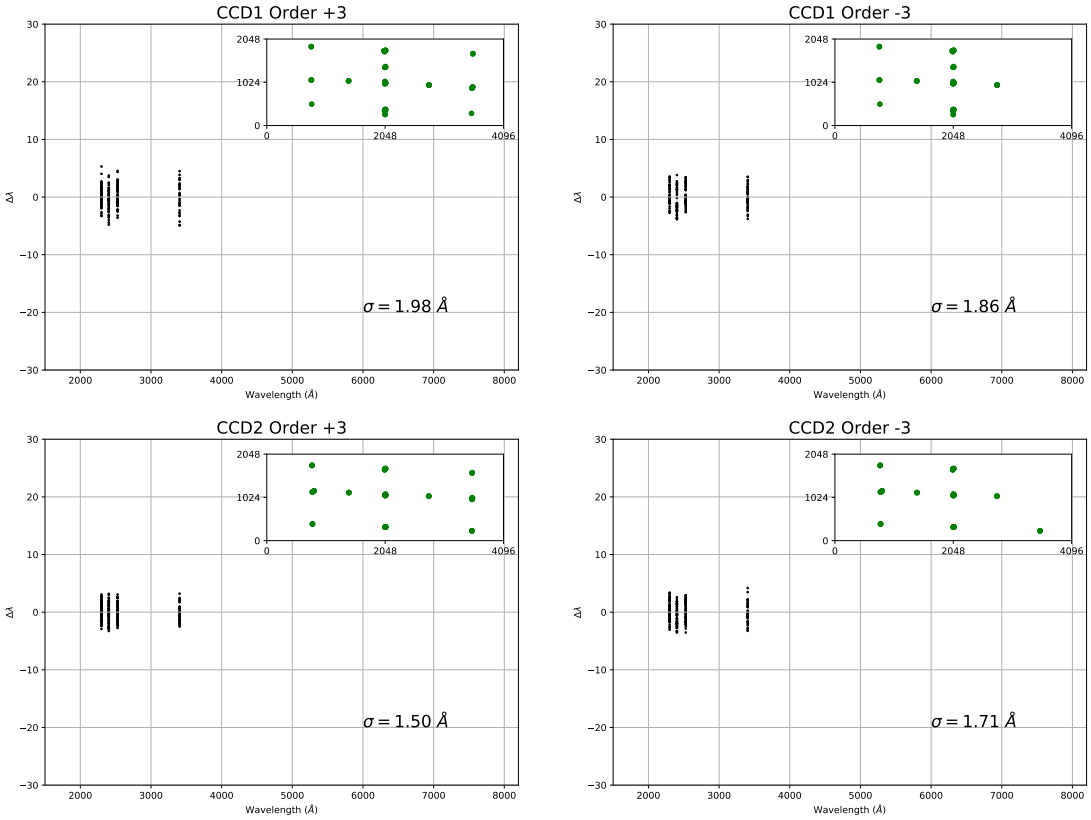

Fig. 12.—: The residuals of our new field dependent wavelength calibration, shown as a function of wavelength of the short ±3 orders. The inset plot shows the location on the detectors where the wavelength was calibrated.

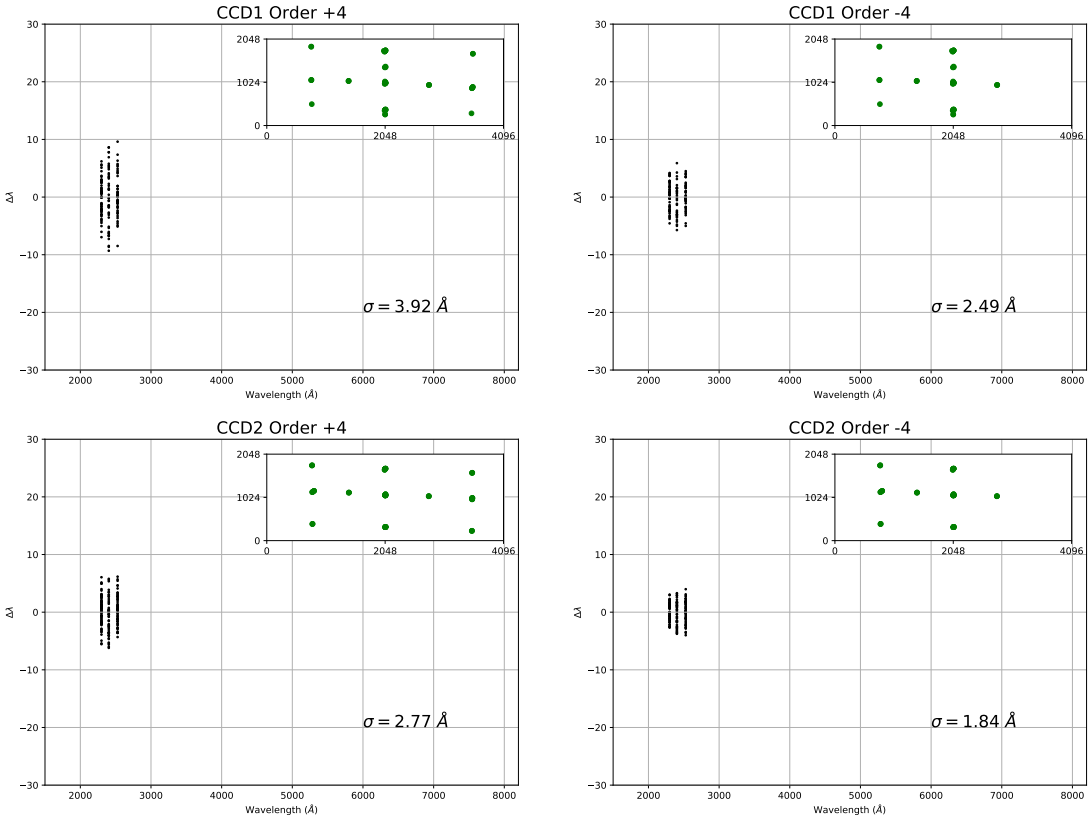

Fig. 13.—: The residuals of our new field dependent wavelength calibration, shown as a function of wavelength of the short ±4 orders.The inset plot shows the location on the detectors where the wavelength was calibrated.

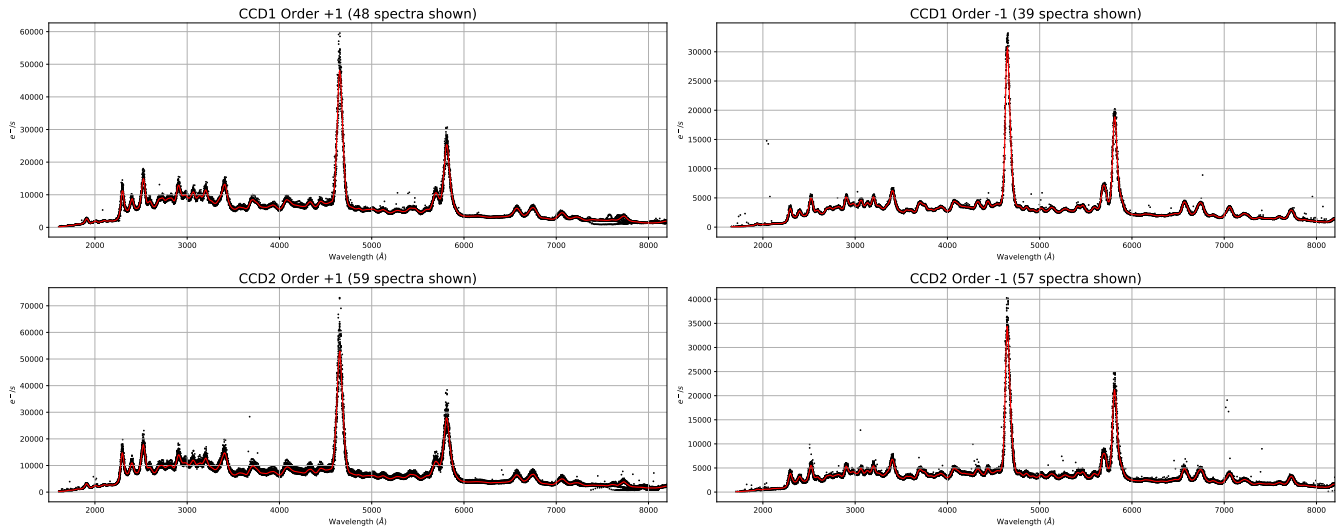

Fig. 14.—: Extracted and wavelength calibrated ±1 order spectra of WR-14 (black dots). We show the mean spectrum in red. Although we show over 50 spectra in each panel, corresponding to different positions on the detector, the extracted spectra match very well with a wavelength calibration error typically much smaller than a pixel, consistent with what we showed in Figure 10)

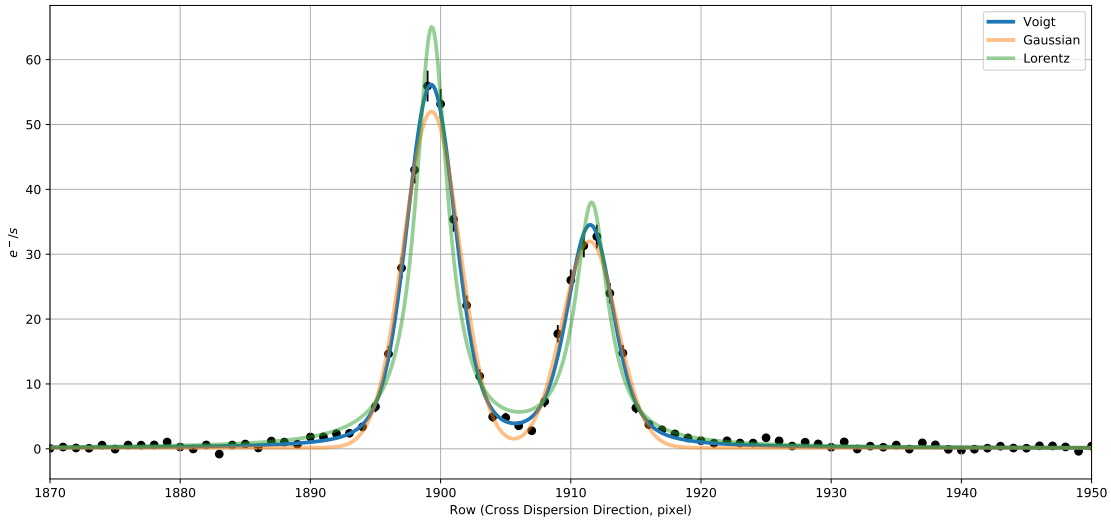

Fig. 15.—: Fit of a $+1^{st}$ and $+2^{nd}$ cross dispersion profile of one of our observations of the flux calibrator GD-71. We obtained a better fit when using a Voigt profile than when using a Gaussian or a Lorentz profile.

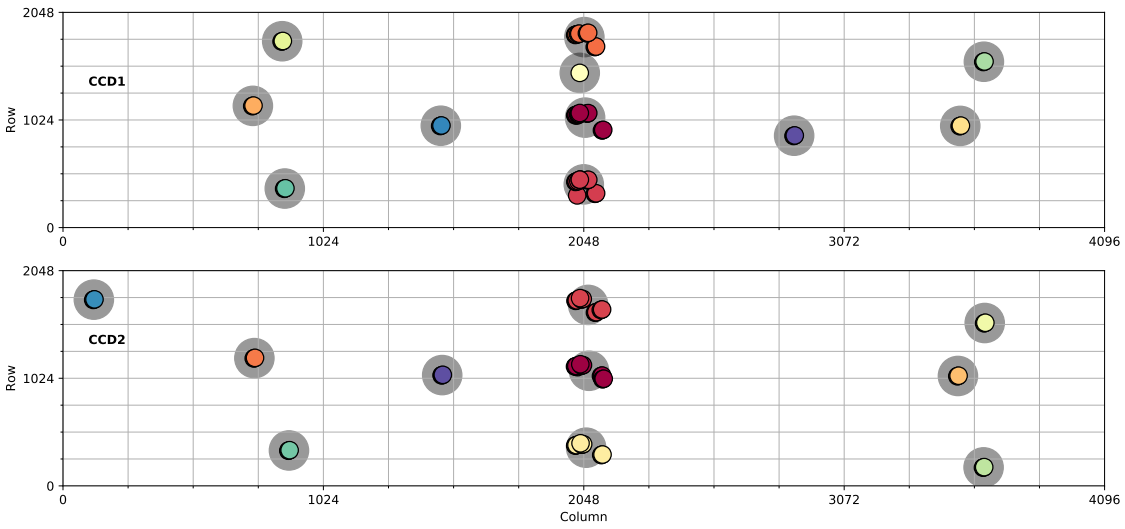

Fig. 16.—: Positions in each detector where the spectra of the flux calibrator GD-71 were individually extracted (smaller colored circles) and and median combined together (larger grey circles)

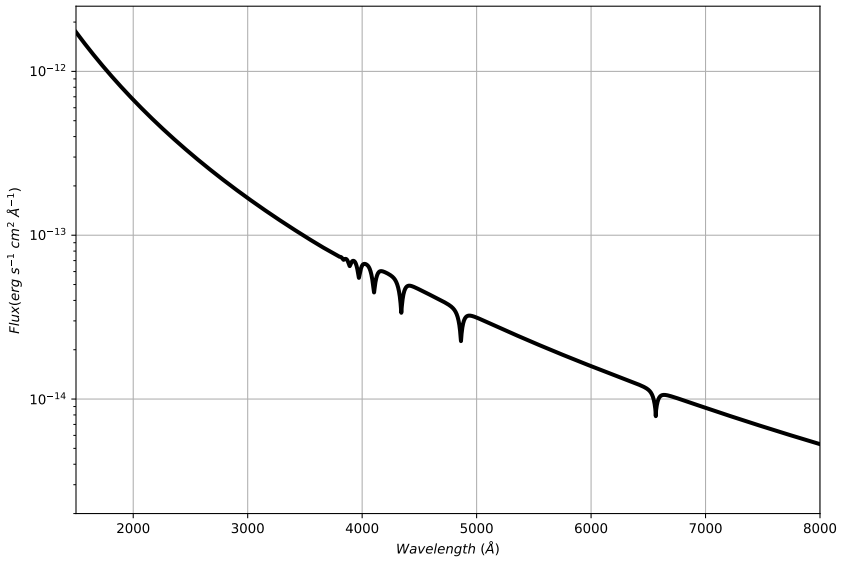

Fig. 17.—: The reference spectrum of GD-71 from CALSPEC (Bohlin et al. 2014) that was used to derive sensitivity estimates of the G280 spectral orders.

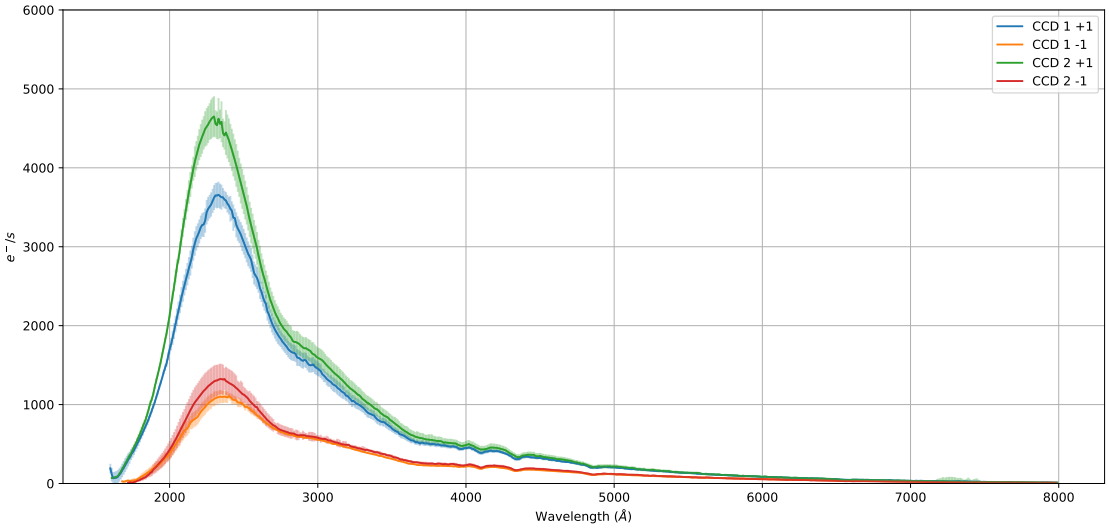

Fig. 18.—: Extracted positive and negative 1^{st} order spectra of GD-71 as measured on CCD1 and CCD2. These measurements were performed at the discrete locations shown in Figure 16 and the error bars reflect the field variation of this spectral order.

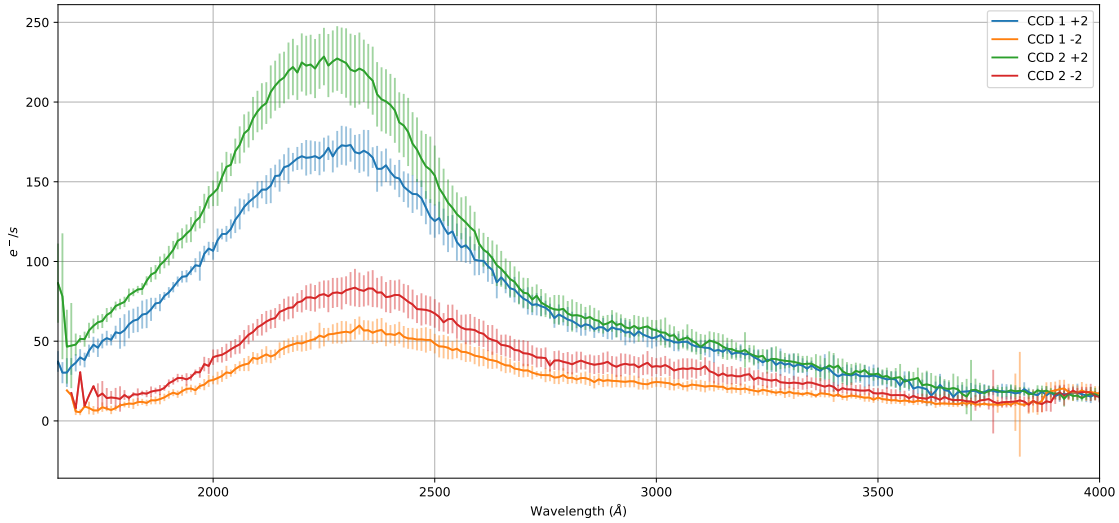

Fig. 19.—: Extracted positive and negative 2^{nd} order spectra of GD-71 as measured on CCD1 and CCD2. These measurements were performed at the discrete locations shown in Figure 16 and the error bars reflect the field variation of this spectral order.

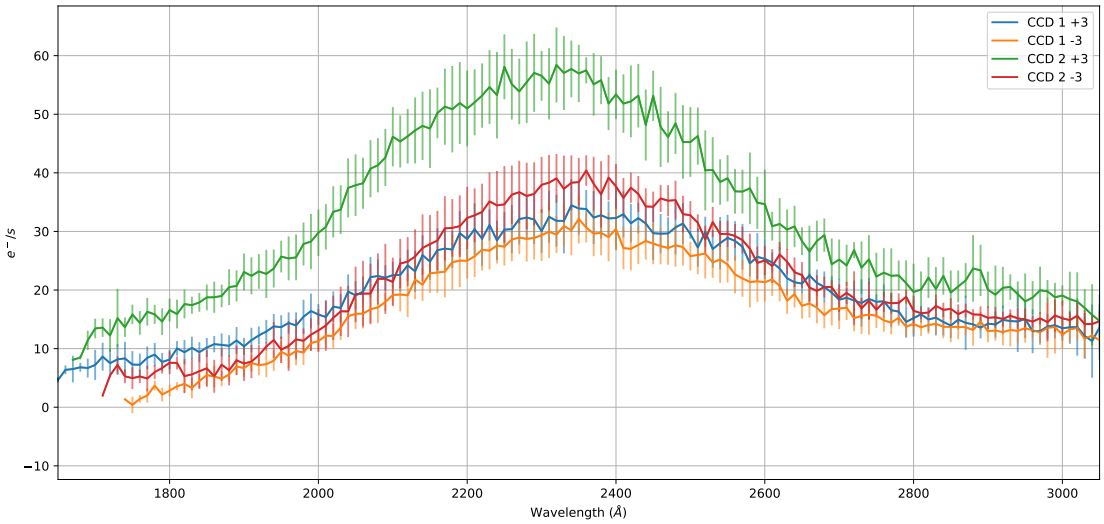

Fig. 20.—: Extracted positive and negative 3^{rd} order spectra of GD-71 as measured on CCD1 and CCD2. These measurements were performed at the discrete locations shown in Figure 16 and the error bars reflect the field variation of this spectral order.

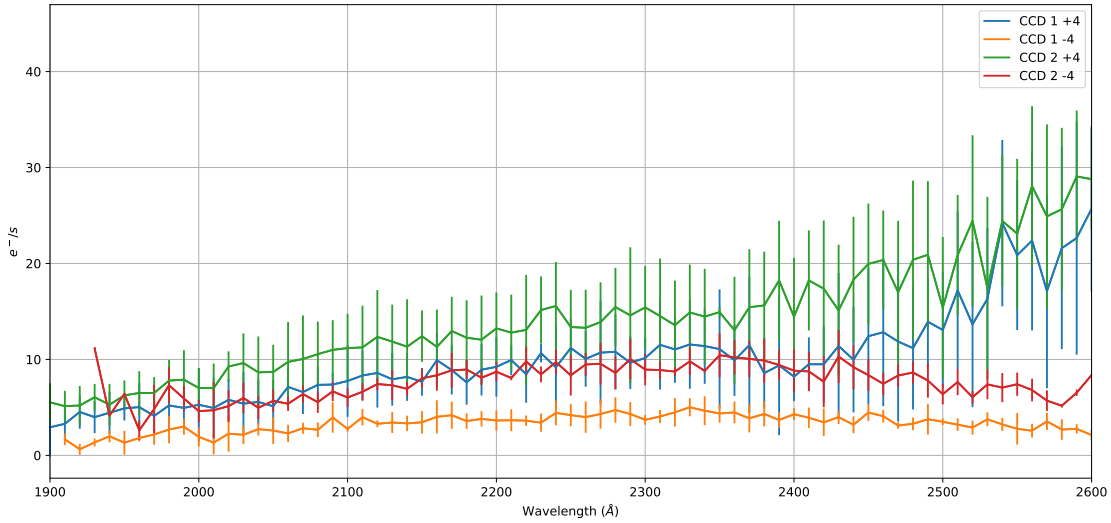

Fig. 21.—: Extracted positive and negative 2^{nd} order spectra of GD-71 as measured on CCD1 and CCD2. These measurements were performed at the discrete locations shown in Figure 16 and the error bars reflect the field variation of this spectral order.

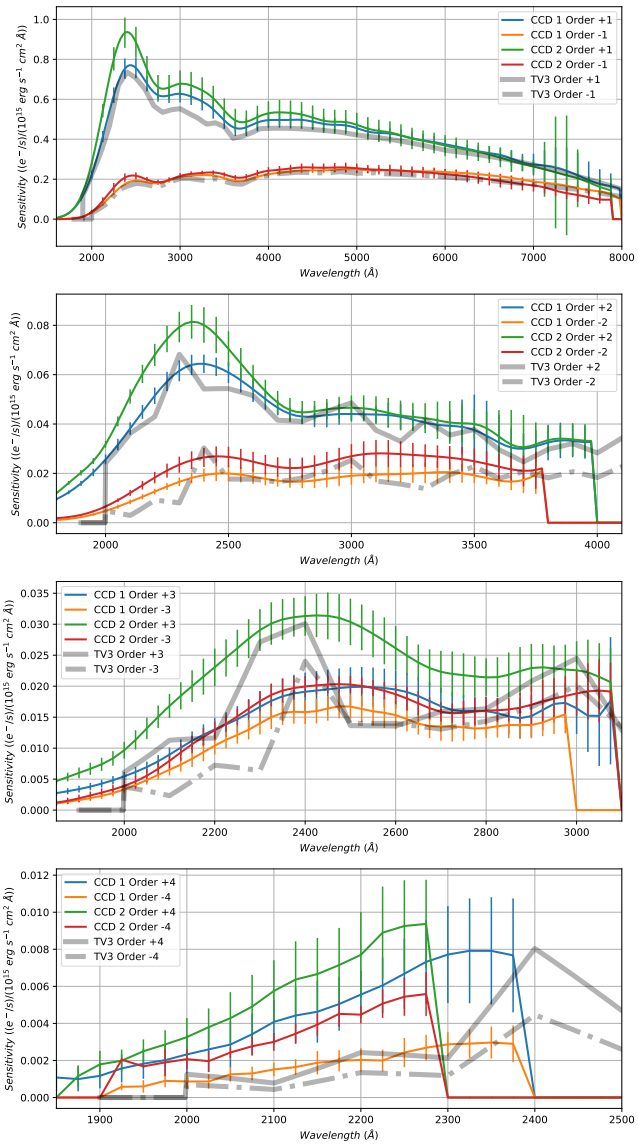

Fig. 22.—: Estimates of the sensitivities of each of the 8 orders we empirically derived using observations of WR14 (colored). We also plot the older, ground based estimates (gray), which were obtained using a monochromator.

REFERENCES

Bohlin, R. C., Gordon, K. D., & Tremblay, P.-E. 2014, PASP, 126, 711. doi:10.1086/677655

Crowther, P. A., Dessart, L., Hillier, D. J., Abbott, J. B., & Fullerton, A. W. 2002, A&A, 392, 653

Kuntschner H., Bushouse H., Kümmel M., Walsh J. R., *The ground calibrations of the WFC3/UVIS G280 grism*, WFC3-2009-01

Pirzkal, N., R. Ryan, and G. Brammer, *Trace and Wavelength Calibrations of the WFC3 G102 and G141 IR Grisms*, WFC3-2016-15

Pirzkal, N., R. Ryan *A More Generalized Coordinate Transformation Approach for Grisms*, WFC3-2017-01

Pirzkal, N., R. Ryan, and B. Rothberg, *Trace and Wavelength Calibrations of the UVIS G280 +1/-1 Grism*, WFC3-2017-20

Rothberg, B., Pirzkal, N., Baggett, S., *ISR 2011-18: First Results from Contamination Monitoring with the WFC3 UVIS G280 Grism*

Willis, A. J., van der Hucht, K. A., Conti, P. S., & Garmany, D. 1986, A&AS, 63, 417

8. Acknowledgments

We thank Jay Anderson for carefully reviewing this document.

9. Appendix

Configuration files were created in the format described in Section 5 of Pirzkal et al. 2016-05. We reproduce the content of the configuration files here, showing the values of the individual 2D polynomial parameters for DISPX, DISPY, and DISPL.

9.A. CCD1

```
# UVIS Configuration file 11/2/2021.
NAXIS 4096 2048
# Order +1
BEAM_+1
DISPL_+1_0 1.247907e+03 1.715171e-01 4.014437e-01 4.606080e-06 -2.067114e-04 1.051219e-05
DISPL_+1_1 1.618352e+04 -5.257680e+00 -1.241063e+01 -8.086326e-05 6.308400e-03 -2.608619e-04
DISPL_+1_2 -9.403328e+04 5.215320e+01 1.138204e+02 2.302944e-04 -5.746772e-02 1.580457e-03
DISPL_+1_3 3.699163e+05 -1.957630e+02 -4.178535e+02 1.600510e-04 2.091686e-01 -3.993138e-03
DISPL_+1_4 -5.922965e+05 3.075212e+02 6.488591e+02 -1.038922e-03 -3.231617e-01 4.620623e-03
DISPL_+1_5 3.277295e+05 -1.682244e+02 -3.539009e+02 6.380609e-04 1.757735e-01 -2.072159e-03
DISPX_+1_0 1.000000e+01
DISPX_+1_1 -5.700000e+02
DISPY_+1_0 1.991281e+02 -2.073556e-03 7.069947e-03 7.430371e-08 -5.304913e-07 -1.286096e-06
DISPY_+1_1 -1.766230e+02 -4.297293e-02 -1.854369e-01 2.078917e-06 4.561426e-05 4.474414e-05
DISPY_+1_2 9.646943e+01 3.552698e-01 1.989722e+00 -1.063473e-05 -5.489048e-04 -4.790314e-04
DISPY_+1_3 2.448071e+03 -1.083281e+00 -9.225543e+00 6.593498e-05 3.044477e-03 2.626904e-03
DISPY_+1_4 -9.312729e+03 9.810426e-01 1.987687e+01 -5.298376e-04 -9.131209e-03 -8.037482e-03
DISPY_+1_5 1.732954e+04 2.076095e+00 -1.274858e+01 2.099644e-03 1.501813e-02 1.349792e-02
DISPY_+1_6 -2.286398e+04 -6.765774e+00 -2.015840e+01 -3.786586e-03 -1.120987e-02 -1.117688e-02
DISPY_+1_7 2.266673e+04 6.634810e+00 2.692799e+01 2.336442e-03 -6.700353e-04 3.283768e-03
DISPY_+1_8 -3.105089e+03 2.521005e+00 1.409290e+01 1.538533e-03 3.064620e-03 -5.739407e-04
DISPY_+1_9 -2.478085e+04 -1.098437e+01 -2.267926e+01 -2.123915e-03 5.377690e-03 1.402719e-03
DISPY_+1_10 1.134289e+04 3.726940e+00 -1.405894e+01 -5.578266e-04 -5.013537e-03 -2.728773e-03
DISPY_+1_11 2.979837e+04 1.156107e+01 1.660022e+01 1.130154e-03 -4.212057e-03 7.544599e-03
DISPY_+1_12 -3.343168e+04 -1.333704e+01 4.525097e+00 9.792405e-05 6.175275e-03 -8.287286e-03
DISPY_+1_13 9.974387e+03 4.360017e+00 -4.950169e+00 -2.623930e-04 -1.940865e-03 2.881733e-03
SENSITIVITY_+1 WFC3.UVIS.G280.CCD1.p1.sens.2021.fits
# Order +2
BEAM_+2
DISPL_+2_0 2.024832e+03 -2.083087e-01 -3.514176e-01 1.358243e-05 1.676521e-04 3.734842e-06
DISPL_+2_1 -1.111281e+03 2.246752e+00 3.163863e+00 -1.426102e-04 -1.627307e-03 1.358261e-05
DISPL_+2_2 1.159132e+04 -6.665012e+00 -9.389449e+00 4.553896e-04 4.905473e-03 -1.097879e-04
DISPL_+2_3 -1.169040e+04 6.977159e+00 9.703328e+00 -4.778925e-04 -5.134452e-03 1.640513e-04
DISPX_+2_0 -1.100000e+02
DISPX_+2_1 -4.400000e+02
DISPY_+2_0 2.041410e+02 -1.035233e-03 5.817347e-03 -4.270251e-07 -3.155895e-07 -9.469504e-07
DISPY_+2_1 -1.508561e+02 -7.765548e-02 5.642477e-02 2.473683e-05 -3.195813e-06 -2.229836e-06
DISPY_+2_2 1.191992e+03 1.319842e+00 -1.778713e+00 -4.181253e-04 1.586993e-04 3.081203e-04
DISPY_+2_3 -6.940575e+03 -1.184139e+01 1.585926e+01 3.396008e-03 -7.767892e-04 -3.469559e-03
DISPY_+2_4 1.969426e+04 5.988403e+01 -6.757421e+01 -1.528851e-02 -7.811398e-04 1.741981e-02
DISPY_+2_5 -2.360021e+04 -1.746648e+02 1.645273e+02 4.041565e-02 1.360129e-02 -4.932173e-02
DISPY_+2_6 -8.948858e+02 2.999207e+02 -2.430514e+02 -6.418066e-02 -3.813870e-02 8.370371e-02
DISPY_+2_7 2.985227e+04 -2.991559e+02 2.167550e+02 6.019354e-02 4.916766e-02 -8.417285e-02
DISPY_+2_8 -2.669085e+04 1.602556e+02 -1.078316e+02 -3.071801e-02 -3.083378e-02 4.612765e-02
DISPY_+2_9 7.517753e+03 -3.563617e+01 2.304743e+01 6.575413e-03 7.602930e-03 -1.059303e-02
SENSITIVITY_+2 WFC3.UVIS.G280.CCD1.p2.sens.2021.fits
# Order +3
BEAM_+3
DISPL_+3_0 1.812834e+03 -8.144435e-02 -1.637695e-01 9.726739e-06 6.464318e-05 1.539862e-05
DISPL_+3_1 5.010111e+02 1.173575e+00 1.677000e+00 -8.702140e-05 -7.949958e-04 -6.536542e-05
DISPL_+3_2 4.678522e+03 -2.560219e+00 -3.966128e+00 1.631260e-04 1.923605e-03 4.478018e-05
DISPX_+3_0 -2.300000e+02
DISPX_+3_1 -5.700000e+02
DISPY_+3_0 2.172404e+02 -4.404165e-03 -2.326764e-03 -5.134273e-08 1.425584e-06 1.380885e-06
DISPY_+3_1 -4.581283e+02 9.622443e-02 3.678026e-01 3.681068e-06 -8.673845e-05 -6.997455e-05
DISPY_+3_2 3.421222e+03 -4.734845e-01 -2.917941e+00 -1.950940e-04 9.067482e-04 2.752907e-04
DISPY_+3_3 -1.077258e+04 -1.583463e+00 7.719787e+00 1.872398e-03 -3.793024e-03 1.281324e-03
DISPY_+3_4 1.084543e+04 1.669144e+01 -2.409367e-01 -7.452941e-03 7.001864e-03 -1.040463e-02
DISPY_+3_5 1.081163e+04 -4.352010e+01 -2.909555e+01 1.434220e-02 -4.830692e-03 2.457058e-02
DISPY_+3_6 -2.778660e+04 4.713105e+01 4.275724e+01 -1.324685e-02 -6.884939e-04 -2.477995e-02
DISPY_+3_7 1.418406e+04 -1.856394e+01 -1.880972e+01 4.716432e-03 1.549921e-03 9.195490e-03
SENSITIVITY_+3 WFC3.UVIS.G280.CCD1.p3.sens.2021.fits
# Order +4
BEAM_+4
DISPL_+4_0 1.600949e+03 1.213913e-01 3.136126e-01 -4.082954e-06 -8.972904e-05 -1.056551e-04
DISPL_+4_1 1.817333e+03 -4.031969e-01 -8.642205e-01 1.656113e-05 3.613914e-04 8.784479e-05
DISPX_+4_0 -4.000000e+02
DISPX_+4_1 -3.000000e+02
DISPY_+4_0 2.104929e+02 4.920439e-05 5.616888e-03 -6.255189e-07 -6.104241e-07 -4.258491e-07
DISPY_+4_1 -1.951789e+02 5.993905e-02 1.968366e-01 -5.779052e-06 -3.044978e-05 -4.909591e-05
DISPY_+4_2 7.748928e+02 -2.793951e-01 -8.528470e-01 3.351429e-05 1.265894e-04 2.197228e-04
DISPY_+4_3 -1.033047e+03 3.729296e-01 1.225291e+00 -5.166284e-05 -1.587204e-04 -3.370864e-04
DISPY_+4_4 4.473251e+02 -1.545797e-01 -5.696233e-01 2.530197e-05 5.909885e-05 1.701652e-04
SENSITIVITY_+4 WFC3.UVIS.G280.CCD1.p4.sens.2021.fits
NAXIS 4096 2048
```

```
# Order -1
BEAM_-1
DISPL_-1_0 1.549674e+03 1.120420e-01 6.417442e-02 -6.147326e-06 -5.088009e-05 -6.847407e-06
DISPL_-1_1 1.186988e+04 -1.247266e+00 -1.489307e+00 1.672497e-04 6.572729e-04 1.935824e-04
DISPL_-1_2 -2.577440e+04 1.205035e+01 1.368945e+01 -1.581738e-03 -6.179599e-03 -1.627053e-03
DISPL_-1_3 8.319987e+04 -4.474023e+01 -5.213631e+01 6.030946e-03 2.308910e-02 5.859683e-03
DISPL_-1_4 -1.213524e+05 7.031003e+01 8.197330e+01 -9.726034e-03 -3.591739e-02 -8.986659e-03
DISPL_-1_5 6.407654e+04 -3.890405e+01 -4.493107e+01 5.525686e-03 1.956408e-02 4.864258e-03
DISPX_-1_0 2.300000e+02
DISPX_-1_1 5.500000e+02
DISPY_-1_0 1.883974e+02 -3.754053e-03 4.924201e-03 4.759416e-08 4.362399e-08 -5.989863e-07
DISPY_-1_1 -6.130667e+02 -1.969040e-02 -9.794328e-02 6.600423e-06 -5.357835e-06 4.602359e-05
DISPY_-1_2 5.133404e+03 8.342800e-01 9.635349e-01 -8.604600e-05 1.535844e-04 -6.630445e-04
DISPY_-1_3 -2.799575e+04 -8.547256e+00 -4.471710e+00 2.591853e-04 -1.450286e-03 4.078690e-03
DISPY_-1_4 9.442694e+04 4.275522e+01 1.093902e+01 1.520206e-03 7.474118e-03 -1.243920e-02
DISPY_-1_5 -1.917375e+05 -1.189323e+02 -1.818947e+01 -1.329702e-02 -2.470405e-02 1.661289e-02
DISPY_-1_6 2.048276e+05 1.863674e+02 3.463798e+01 3.979646e-02 5.482801e-02 8.509309e-03
DISPY_-1_7 -2.557173e+04 -1.462479e+02 -6.273186e+01 -5.463689e-02 -7.985152e-02 -7.105488e-02
DISPY_-1_8 -2.090328e+05 1.741713e+01 4.420711e+01 1.989377e-02 7.204076e-02 1.215042e-01
DISPY_-1_9 2.294532e+05 6.065767e+01 6.153437e+01 3.378501e-02 -4.029665e-02 -8.961658e-02
DISPY_-1_10 -4.953257e+04 -5.494505e+01 -1.473389e+02 -3.499904e-02 2.495390e-02 -9.630011e-03
DISPY_-1_11 -7.353620e+04 3.781011e+01 1.145701e+02 -2.604193e-03 -2.728788e-02 7.108235e-02
DISPY_-1_12 5.672844e+04 -2.437575e+01 -3.811669e+01 1.581248e-02 1.925721e-02 -5.054049e-02
DISPY_-1_13 -1.261501e+04 7.228475e+00 4.082948e+00 -5.450909e-03 -5.111253e-03 1.211345e-02
SENSITIVITY_-1 WFC3.UVIS.G280.CCD1.m1.sens.2021.fits
# Order -2
BEAM_-2
DISPL_-2_0 1.663849e+03 4.262151e-02 -8.425576e-03 1.089535e-06 -1.426305e-05 -3.244403e-06
DISPL_-2_1 4.192888e+03 1.979919e-01 3.280327e-01 6.240839e-06 -1.375091e-04 3.001150e-05
DISPL_-2_2 1.737929e+03 -7.388151e-01 -2.889202e+00 -3.364382e-04 1.245910e-03 -2.124256e-06
DISPL_-2_3 -2.465904e+03 -1.462081e+00 4.509130e+00 1.522150e-03 -2.077705e-03 -2.861282e-05
DISPX_-2_0 3.500000e+02
DISPX_-2_1 5.500000e+02
DISPY_-2_0 1.797632e+02 -3.749091e-03 3.084220e-03 7.811054e-08 -1.498714e-09 7.437671e-08
DISPY_-2_1 -2.849476e+02 -7.426225e-04 -4.874903e-02 8.816693e-06 -2.309535e-05 3.468432e-05
DISPY_-2_2 1.119395e+03 1.476601e-01 3.157227e-01 -1.268492e-04 4.291934e-04 -4.920665e-04
DISPY_-2_3 -3.115988e+03 -1.310789e+00 -5.050898e-01 7.984248e-04 -3.106123e-03 2.870848e-03
DISPY_-2_4 5.305771e+03 5.521898e+00 -2.561995e+00 -2.763279e-03 1.233817e-02 -9.297641e-03
DISPY_-2_5 -5.883628e+03 -1.241353e+01 1.267715e+01 5.621050e-03 -2.991129e-02 1.911526e-02
DISPY_-2_6 6.250749e+03 1.460777e+01 -2.371703e+01 -6.667333e-03 4.527629e-02 -2.601262e-02
DISPY_-2_7 -7.902364e+03 -7.555967e+00 2.328939e+01 4.278266e-03 -4.162732e-02 2.253373e-02
DISPY_-2_8 6.714891e+03 1.409697e-01 -1.221075e+01 -1.193608e-03 2.123268e-02 -1.106200e-02
DISPY_-2_9 -2.260354e+03 8.597784e-01 2.751915e+00 4.486396e-05 -4.605215e-03 2.309556e-03
SENSITIVITY_-2 WFC3.UVIS.G280.CCD1.m2.sens.2021.fits
# Order -3
BEAM_-3
DISPL_-3_0 1.699096e+03 4.791965e-02 5.768717e-03 1.349425e-06 -1.796410e-05 2.700630e-06
DISPL_-3_1 2.241699e+03 -5.076667e-03 -6.030019e-02 -9.272839e-06 3.117269e-05 -9.086008e-06
DISPL_-3_2 -1.272566e+02 1.978762e-02 2.508017e-02 8.402054e-06 -2.274952e-05 7.800285e-06
DISPX_-3_0 4.750000e+02
DISPX_-3_1 4.250000e+02
DISPY_-3_0 1.644988e+02 -4.179673e-04 3.403746e-03 -1.212223e-07 -1.044905e-06 5.146071e-07
DISPY_-3_1 -4.224046e+01 -5.480477e-02 -1.330544e-02 6.772708e-06 7.612704e-06 -2.465134e-06
DISPY_-3_2 -3.205220e+02 3.687420e-01 -1.468771e-01 -4.071000e-05 2.743191e-05 1.537238e-05
DISPY_-3_3 1.358063e+03 -1.179057e+00 1.361773e+00 9.840595e-05 -3.192360e-04 -1.596528e-04
DISPY_-3_4 -2.606893e+03 2.237403e+00 -4.580686e+00 -1.216446e-04 9.657522e-04 7.606344e-04
DISPY_-3_5 2.803869e+03 -2.708439e+00 7.477189e+00 1.053406e-04 -1.336005e-03 -1.593903e-03
DISPY_-3_6 -1.690183e+03 1.939120e+00 -5.910014e+00 -8.518050e-05 8.800377e-04 1.490757e-03
DISPY_-3_7 4.614511e+02 -6.149833e-01 1.806220e+00 3.882204e-05 -2.208068e-04 -5.133015e-04
SENSITIVITY_-3 WFC3.UVIS.G280.CCD1.m3.sens.2021.fits
# Order -4
BEAM_-4
DISPL_-4_0 1.842831e+03 7.204487e-02 2.150832e-02 -2.672041e-06 -2.824821e-05 4.433913e-06
DISPL_-4_1 1.468023e+03 -8.327019e-02 -1.233711e-01 1.624981e-06 6.942547e-05 -1.145358e-05
DISPX_-4_0 6.400000e+02
DISPX_-4_1 3.500000e+02
DISPY_-4_0 1.514997e+02 -3.560823e-03 3.106131e-03 3.759473e-07 -4.151129e-08 -7.577361e-07
DISPY_-4_1 -3.441476e+01 8.765370e-03 -4.449884e-02 -5.821345e-06 6.682905e-06 1.338941e-05
DISPY_-4_2 -9.380154e+01 1.014785e-02 1.131061e-01 1.985179e-05 -5.029344e-05 -1.161397e-05
DISPY_-4_3 2.265722e+02 -6.508698e-02 -8.721553e-02 -2.932264e-05 1.178812e-04 -5.373507e-05
DISPY_-4_4 -1.448692e+02 4.896433e-02 1.273369e-02 1.585546e-05 -7.752604e-05 5.724802e-05
SENSITIVITY_-4 WFC3.UVIS.G280.CCD1.m4.sens.2021.fits
```

9.B. CCD2

```
# UVIS Configuration file 11/2/2021. N. Pirzkal WFC3-ISR-XXX
NAXIS 4096 2048
# Order +1
BEAM_+1
DISPL_+1_0 1.630589e+03 -1.356638e-02 -4.836527e-02 2.154176e-06 8.866305e-06 2.217574e-05
DISPL_+1_1 4.359513e+03 5.023372e-01 1.300742e+00 -3.364980e-05 -2.465696e-04 -6.271406e-04
DISPL_+1_2 1.850520e+04 -2.617759e+00 -1.291570e+01 2.616000e-04 2.236313e-03 5.925140e-03
DISPL_+1_3 -4.765252e+04 8.552874e+00 4.829397e+01 -8.372390e-04 -8.166799e-03 -2.245505e-02
DISPL_+1_4 6.073157e+04 -1.231319e+01 -7.747520e+01 1.108031e-03 1.278223e-02 3.651968e-02
DISPL_+1_5 -2.984475e+04 6.402318e+00 4.454563e+01 -5.062703e-04 -7.182101e-03 -2.125603e-02
DISPX_+1_0 1.000000e+01
DISPX_+1_1 -5.700000e+02
DISPY_+1_0 1.972287e+02 -1.607829e-03 2.153677e-03 -6.423415e-08 8.998062e-08 -1.428478e-07
DISPY_+1_1 -3.350614e+02 -2.075852e-02 2.139390e-02 3.605910e-06 -3.179437e-06 6.399737e-07
DISPY_+1_2 1.391344e+03 2.415808e-01 -1.575573e-01 -3.505967e-05 2.349381e-05 -6.585515e-06
DISPY_+1_3 -2.359703e+03 -1.037057e+00 6.504751e-01 1.546831e-04 -9.051664e-05 1.357855e-04
DISPY_+1_4 -1.242211e+03 1.891149e+00 -1.804593e+00 -3.931127e-04 2.550381e-04 -9.357880e-04
DISPY_+1_5 1.236114e+04 -8.243365e-01 4.695995e+00 7.479311e-04 -5.280565e-04 3.033951e-03
DISPY_+1_6 -1.946290e+04 -1.473860e+00 -9.364401e+00 -1.131641e-03 1.599879e-04 -5.042447e-03
DISPY_+1_7 7.553411e+03 9.786248e-01 7.996849e+00 8.604098e-04 1.808640e-03 3.572340e-03
DISPY_+1_8 9.449305e+03 1.513346e+00 4.334242e+00 2.636880e-04 -2.287931e-03 8.975291e-04
DISPY_+1_9 -6.527736e+03 -2.673097e+00 -9.859942e+00 -4.972459e-04 -1.911058e-03 -2.121382e-03
DISPY_+1_10 -4.955326e+03 3.313298e+00 -2.917805e+00 -2.844164e-04 3.679248e-03 -1.754378e-03
DISPY_+1_11 3.428637e+03 -2.850438e+00 1.275796e+01 -4.449199e-05 1.514325e-03 4.305526e-03
DISPY_+1_12 2.102848e+03 8.724013e-01 -7.703790e+00 7.237847e-04 -4.349664e-03 -2.632501e-03
DISPY_+1_13 -1.426592e+03 7.032685e-02 1.362010e+00 -3.679957e-04 1.727959e-03 5.455627e-04
SENSITIVITY_+1 WFC3.UVIS.G280.CCD2.p1.sens.2021.fits
# Order +2
BEAM_+2
DISPL_+2_0 1.676118e+03 -3.536551e-03 -4.767630e-02 3.123565e-06 4.997100e-06 1.425205e-05
DISPL_+2_1 2.248999e+03 3.096268e-01 5.708216e-01 -4.696180e-05 -7.354401e-05 -2.140630e-04
DISPL_+2_2 2.174241e+03 -9.686019e-01 -2.395528e+00 1.881956e-04 2.788000e-04 8.677878e-04
DISPL_+2_3 -1.933271e+03 1.050699e+00 2.555187e+00 -2.090548e-04 -2.859473e-04 -9.403175e-04
DISPX_+2_0 -1.100000e+02
DISPX_+2_1 -4.400000e+02
DISPY_+2_0 1.993287e+02 -2.406869e-03 3.143182e-03 1.035738e-08 8.516950e-08 -1.222680e-07
DISPY_+2_1 -1.502112e+02 -2.204522e-03 2.016442e-02 6.053318e-07 -3.189711e-06 -3.022678e-06
DISPY_+2_2 3.357689e+02 9.488519e-02 -8.142861e-02 -3.610237e-06 -6.943536e-07 1.493979e-05
DISPY_+2_3 7.148597e+02 -9.972004e-01 -5.434463e-01 5.384257e-06 2.901583e-04 1.669835e-04
DISPY_+2_4 -8.525038e+03 5.293798e+00 5.356826e+00 8.945988e-05 -2.163623e-03 -1.359350e-03
DISPY_+2_5 3.042348e+04 -1.508498e+01 -1.692352e+01 -7.086295e-04 7.307462e-03 3.450163e-03
DISPY_+2_6 -5.726521e+04 2.394687e+01 2.603967e+01 2.187123e-03 -1.355361e-02 -3.003702e-03
DISPY_+2_7 6.040546e+04 -2.115000e+01 -2.059891e+01 -3.283710e-03 1.432401e-02 -1.088940e-03
DISPY_+2_8 -3.374909e+04 9.687638e+00 7.658352e+00 2.383888e-03 -8.126292e-03 3.138077e-03
DISPY_+2_9 7.785238e+03 -1.785537e+00 -9.155935e-01 -6.707601e-04 1.924652e-03 -1.318418e-03
SENSITIVITY_+2 WFC3.UVIS.G280.CCD2.p2.sens.2021.fits
# Order +3
BEAM_+3
DISPL_+3_0 1.671077e+03 1.573278e-02 -2.205783e-02 2.785193e-07 2.116073e-06 3.115113e-06
DISPL_+3_1 2.442687e+03 7.880383e-02 4.326069e-02 -3.692789e-06 -1.806423e-05 -1.181856e-05
DISPL_+3_2 1.884717e+02 -1.975992e-02 -5.834427e-02 9.590756e-07 1.547900e-05 7.359638e-06
DISPX_+3_0 -2.300000e+02
DISPX_+3_1 -5.700000e+02
DISPY_+3_0 2.033447e+02 -3.003634e-03 3.803506e-03 1.207644e-07 1.089079e-08 4.900511e-08
DISPY_+3_1 -1.649310e+02 3.096656e-02 1.233238e-02 -5.956789e-06 3.291009e-06 -1.016144e-05
DISPY_+3_2 1.070481e+03 -4.781166e-01 -7.042097e-02 1.022311e-04 -8.905126e-05 2.078745e-04
DISPY_+3_3 -5.726498e+03 3.252517e+00 4.773413e-01 -6.833943e-04 6.193857e-04 -1.590647e-03
DISPY_+3_4 1.848792e+04 -1.073396e+01 -2.501803e+00 2.186649e-03 -1.834956e-03 5.888249e-03
DISPY_+3_5 -3.231911e+04 1.827168e+01 6.920774e+00 -3.582491e-03 2.528083e-03 -1.129088e-02
DISPY_+3_6 2.827470e+04 -1.541803e+01 -8.788156e+00 2.886838e-03 -1.488886e-03 1.075072e-02
DISPY_+3_7 -9.681377e+03 5.087383e+00 4.061726e+00 -9.009449e-04 2.392882e-04 -3.999961e-03
SENSITIVITY_+3 WFC3.UVIS.G280.CCD2.p3.sens.2021.fits
# Order +4
BEAM_+4
DISPL_+4_0 1.962114e+03 -3.453827e-02 -1.256688e-01 8.981131e-06 1.262681e-05 4.438854e-05
DISPL_+4_1 7.062482e+02 1.953781e-01 2.345697e-01 -3.021334e-05 -2.122666e-05 -1.047322e-04
DISPX_+4_0 -4.000000e+02
DISPX_+4_1 -3.000000e+02
DISPY_+4_0 1.990865e+02 -1.026975e-03 4.417462e-03 -2.649168e-07 3.088567e-07 -1.259228e-07
DISPY_+4_1 -1.547422e+01 -2.748205e-03 1.170829e-02 1.235218e-06 -5.603464e-06 9.183093e-07
DISPY_+4_2 2.964181e+00 -2.405694e-02 -1.881920e-02 3.613584e-06 2.007121e-05 -7.310822e-06
DISPY_+4_3 -6.629839e+01 1.173103e-01 5.842435e-02 -2.375969e-05 -1.769133e-05 -2.727244e-05
DISPY_+4_4 7.804762e+01 -9.522696e-02 -6.990068e-02 1.988638e-05 4.476990e-06 4.361175e-05
SENSITIVITY_+4 WFC3.UVIS.G280.CCD2.p4.sens.2021.fits
NAXIS 4096 2048
```

```
# Order -1
BEAM_-1
DISPL_-1_0 1.710584e+03 5.788712e-02 2.596822e-02 -2.577369e-06 -4.151712e-06 -2.717395e-05
DISPL_-1_1 1.064077e+04 -1.217292e-01 -1.266736e+00 1.662175e-05 7.604819e-05 5.313516e-04
DISPL_-1_2 -1.216808e+04 1.217738e+00 9.052713e+00 -1.205445e-04 -6.782489e-04 -3.985724e-03
DISPL_-1_3 3.013892e+04 -3.467332e+00 -2.919329e+01 4.236397e-04 2.445740e-03 1.276931e-02
DISPL_-1_4 -3.701859e+04 5.327609e+00 4.219600e+01 -7.792730e-04 -3.908885e-03 -1.828681e-02
DISPL_-1_5 1.777832e+04 -3.255826e+00 -2.240687e+01 5.390166e-04 2.266093e-03 9.598347e-03
DISPX_-1_0 2.300000e+02
DISPX_-1_1 5.500000e+02
DISPY_-1_0 1.842402e+02 -5.748613e-03 5.306088e-03 2.423096e-07 -8.167272e-09 -7.121788e-07
DISPY_-1_1 -6.863071e+02 7.215000e-02 -9.501876e-02 1.270610e-06 -7.861798e-06 2.106261e-05
DISPY_-1_2 6.702849e+03 -4.283056e-01 1.152883e+00 -7.885701e-05 1.727686e-04 -2.082361e-04
DISPY_-1_3 -4.051184e+04 -2.005410e-01 -8.198870e+00 7.010484e-04 -1.385623e-03 6.756200e-04
DISPY_-1_4 1.480792e+05 1.254841e+01 3.577548e+01 -2.076648e-03 5.435539e-03 1.234730e-03
DISPY_-1_5 -3.290458e+05 -5.708126e+01 -9.523299e+01 -1.602102e-03 -1.099893e-02 -1.532593e-02
DISPY_-1_6 4.240330e+05 1.175750e+02 1.445581e+02 2.480890e-02 9.391646e-03 4.521843e-02
DISPY_-1_7 -2.432740e+05 -1.124889e+02 -9.868595e+01 -6.291065e-02 5.339779e-03 -5.318857e-02
DISPY_-1_8 -8.620871e+04 2.374968e+01 -1.468743e+01 6.843248e-02 -2.398854e-02 -9.316990e-03
DISPY_-1_9 2.018572e+05 2.395379e+01 5.466148e+01 -1.807181e-02 3.275108e-02 8.566366e-02
DISPY_-1_10 -3.750273e+04 1.982945e+01 -2.427389e+01 -2.854545e-02 -2.636399e-02 -6.189288e-02
DISPY_-1_11 -1.150540e+05 -4.741698e+01 2.649183e+01 2.475643e-02 1.050800e-02 -2.243102e-02
DISPY_-1_12 9.612970e+04 2.227079e+01 -3.477823e+01 -4.599250e-03 3.692984e-04 4.379005e-02
DISPY_-1_13 -2.457625e+04 -2.387749e+00 1.331722e+01 -8.146030e-04 -1.219466e-03 -1.424619e-02
SENSITIVITY_-1 WFC3.UVIS.G280.CCD2.m1.sens.2021.fits
# Order -2
BEAM_-2
DISPL_-2_0 2.043241e+03 -1.338155e-01 -2.967159e-01 2.164434e-05 7.003060e-05 4.375142e-05
DISPL_-2_1 6.515535e+02 2.182778e+00 3.596334e+00 -2.672740e-04 -9.133266e-04 -6.337219e-04
DISPL_-2_2 1.343817e+04 -7.172036e+00 -1.387958e+01 7.533050e-04 3.338535e-03 2.559270e-03
DISPL_-2_3 -1.464216e+04 6.139328e+00 1.581138e+01 -3.307049e-04 -3.449745e-03 -3.168036e-03
DISPX_-2_0 3.500000e+02
DISPX_-2_1 5.500000e+02
DISPY_-2_0 1.766659e+02 -4.434826e-03 3.338505e-03 2.238570e-07 3.048554e-08 -5.905823e-07
DISPY_-2_1 -2.276769e+02 1.214989e-02 -1.797400e-01 -5.502683e-06 1.305976e-05 7.417242e-05
DISPY_-2_2 -3.562857e+02 2.956758e-02 4.173926e+00 1.576390e-04 -3.603130e-04 -1.780431e-03
DISPY_-2_3 1.202096e+04 -2.624622e-02 -4.031611e+01 -1.852164e-03 3.682920e-03 1.712528e-02
DISPY_-2_4 -7.122950e+04 -2.613364e+00 1.983158e+02 1.047624e-02 -1.866914e-02 -8.370758e-02
DISPY_-2_5 2.109084e+05 1.399330e+01 -5.494697e+02 -3.221656e-02 5.289143e-02 2.304915e-01
DISPY_-2_6 -3.553112e+05 -3.081669e+01 8.921365e+02 5.669512e-02 -8.786195e-02 -3.717986e-01
DISPY_-2_7 3.451827e+05 3.360310e+01 -8.407952e+02 -5.687920e-02 8.511729e-02 3.477473e-01
DISPY_-2_8 -1.802851e+05 -1.768588e+01 4.256016e+02 3.017164e-02 -4.455911e-02 -1.744029e-01
DISPY_-2_9 3.923274e+04 3.514006e+00 -8.945102e+01 -6.550309e-03 9.743709e-03 3.624472e-02
SENSITIVITY_-2 WFC3.UVIS.G280.CCD2.m2.sens.2021.fits
# Order -3
BEAM_-3
DISPL_-3_0 1.459090e+03 1.475280e-01 4.446218e-01 1.420271e-05 -1.609034e-04 -1.082383e-04
DISPL_-3_1 4.378876e+03 -7.950560e-01 -3.001402e+00 -7.792160e-05 1.044163e-03 6.597715e-04
DISPL_-3_2 -3.544333e+03 1.449196e+00 4.360619e+00 5.970065e-05 -1.564150e-03 -8.837899e-04
DISPX_-3_0 4.750000e+02
DISPX_-3_1 4.250000e+02
DISPY_-3_0 1.715060e+02 -4.860941e-03 1.239424e-04 2.154246e-07 7.389488e-07 -4.042887e-07
DISPY_-3_1 -1.529198e+02 6.438630e-03 -1.659110e-02 1.281884e-06 -4.748715e-06 1.951991e-05
DISPY_-3_2 2.112297e+02 1.182573e-01 4.419014e-01 -3.537114e-05 -2.738957e-05 -2.847653e-04
DISPY_-3_3 8.381005e+02 -1.199346e+00 -3.463434e+00 3.117195e-04 4.011466e-04 1.789728e-03
DISPY_-3_4 -5.172124e+03 4.673846e+00 1.209355e+01 -1.238868e-03 -1.610907e-03 -5.605326e-03
DISPY_-3_5 1.080257e+04 -8.925072e+00 -2.108075e+01 2.432960e-03 3.003684e-03 9.127680e-03
DISPY_-3_6 -1.011905e+04 8.191314e+00 1.787319e+01 -2.278017e-03 -2.668860e-03 -7.370292e-03
DISPY_-3_7 3.534080e+03 -2.850468e+00 -5.841811e+00 8.021307e-04 9.037994e-04 2.322964e-03
SENSITIVITY_-3 WFC3.UVIS.G280.CCD2.m3.sens.2021.fits
# Order -4
BEAM_-4
DISPL_-4_0 1.988431e+03 9.631749e-03 -5.837380e-02 3.621213e-06 1.029971e-05 8.823918e-06
DISPL_-4_1 1.223339e+03 7.400493e-02 1.076056e-01 -8.478535e-06 -3.358865e-05 -3.158972e-05
DISPX_-4_0 6.400000e+02
DISPX_-4_1 3.500000e+02
DISPY_-4_0 1.562705e+02 -4.197183e-03 -4.436185e-03 4.154938e-07 2.392727e-07 1.882577e-06
DISPY_-4_1 -7.146658e+01 -4.569027e-03 7.814884e-02 3.379334e-07 2.840931e-06 -3.586340e-05
DISPY_-4_2 6.670463e+01 8.230305e-03 -3.300602e-01 1.214309e-05 -2.500297e-05 1.554824e-04
DISPY_-4_3 -6.308005e+01 6.310511e-02 5.416663e-01 -5.291586e-05 4.315913e-05 -2.542835e-04
DISPY_-4_4 3.580453e+01 -7.523960e-02 -2.993540e-01 4.361409e-05 -2.023828e-05 1.372812e-04
SENSITIVITY_-4 WFC3.UVIS.G280.CCD2.m4.sens.2021.fits
```